ADVANCES IN ATMOSPHERIC SCIENCES, VOL. 24, NO. 5, 2007, 881–892

Impacts of the Thermal Effects of Sub-grid Orography on the Heavy Rainfall Events Along the Yangtze River Valley in 1991

FENG Lei (冯 蕾) and ZHANG Yaocun* (张耀存)

Department of Atmospheric Sciences, Nanjing University, Nanjing 210093

(Received 13 October 2006; revised 16 February 2007)

ABSTRACT

A $P-\sigma$ regional climate model using a parameterization scheme to account for the thermal effects of the sub-grid scale orography was used to simulate the three heavy rainfall events that occurred within the Yangtze River Valley during the mei-yu period of 1991. The simulation results showed that by considering the sub-grid scale topography scheme, one can significantly improve the performance of the model for simulating the rainfall distribution and intensity during these three heavy rainfall events, most especially the second and third. It was also discovered that the rainfall was mainly due to convective precipitation. The comparison between experiments, either with and without the sub-grid scale topography scheme, showed that the model using the scheme reproduced the convergence intensity and distribution at the 850 hPa level and the ascending motion and moisture convergence center located at 500 hPa over the Yangtze River valley. However, some deviations still exist in the simulation of the atmospheric moisture content, the convergence distribution and the moisture transportation route, which mainly result in lower simulated precipitation levels. Further analysis of the simulation results demonstrated that the sub-grid topography scheme modified the distribution of the surface energy budget components, especially at the south and southwest edges of the Tibetan Plateau, leading to the development and eastward propagation of the negative geopotential height difference and positive temperature-lapse rate difference at 700 hPa, which possibly led to an improved precipitation simulation over eastern China.

Key words: sub-grid scale orographic parameterization, heavy rainfall events, numerical simulation

DOI: 10.1007/s00376-007-0881-4

1. Introduction

The spatial heterogeneities of the land surface, such as the surface topography, vegetation and soil categories, play a non-negligible role in regional climate change. They can profoundly change the land-surface energy budget and affect the exchanges of moisture and other elements that occur between the soil and atmosphere. This exchange is due to a series of nonlinear effects, that lead to the adjustment of the atmospheric circulation and finally result in the reallocation of various atmospheric elements. As climate models have developed, research investigating the impact that heterogeneities in the land surface have upon the atmosphere have become a hot topic in recent years, with many studies being carried out in an effort to develop the parameterization scheme of the land surface heterogeneities and incorporate them into available climate models (Giorgi, 1997; Giorgi and Avissar, 1997; Ghan et al., 2002; Seth et al., 1994; Leung and Ghan, 1998). Under this background, some biology-atmosphere-land schemes, such as the Biosphere-Atmosphere Transfer Scheme (BATS) and Community Land Model (CLM), were proposed and then were proved to provide good performance in depicting the impacts of the land-surface soil and vegetation categories on the atmosphere. Nowadays, they are widely used in climate models and further research is ongoing to improve these schemes. At the same time, as the model resolution has increased, people have began to realize that it was feasible and essential to consider the impacts of the sub-grid scale topography on the atmosphere in climate models.

Over the past two decades, some effective parame-

*Corresponding author: ZHANG Yaocun, yczhang@nju.edu.cn

terization schemes for depicting the dynamical effects of the sub-grid scale topography, such as the envelope orography or the orographic gravity-wave-drag parameterization scheme, have been proposed (Wallace et al., 1983; Li and Zhu, 1990; Qian and Dong, 1995; Qian, 2000; Palmer et al., 1986). However, less attention has been paid to the thermal effects of the sub-grid scale orography and only a few studies have to date been carried out (Weng et al., 1984; Fu, 1983; Li and Weng, 1987; Seth et al., 1994; Giorgi et al., 2003). Recently, based on the studies mentioned above, Zhang et al. (2006) and Zhu and Zhang (2005) have completed an effective attempt at depicting the character of the topography by using three major parameters, including the terrain height, slope and orientation and also considered their thermal effects within parameterization scheme. In their studies, this scheme was introduced into the $P-\sigma$ regional climate model in an effort to simulate the regional climate change and evaluate the thermal impacts of the sub-grid scale orography on the surface energy budget over East Asia, by computing the terrain slopes and orientations based on the high-resolution topographic data. The numerical experimental results showed that this scheme could reasonably depict the influence of the sub-grid scale orography on the solar and infrared radiations, as well as on the sensible and latent heat fluxes at the land surface. However, the effect that this scheme has on a specific rainfall event was still unknown.

In this paper, a regional climate model, using the parameterization scheme accounting for the thermal effects of the sub-grid scale orography was used to simulate the heavy rainfall events that occurred within the Yangtze River valley during the mei-yu period of 1991. The model's performance in simulating a specific heavy rainfall event was evaluated by analyzing the impact that the sub-grid topography scheme had upon the vertical motion, moisture condition and other atmospheric conditions.

This paper is organized as follows: section 2 gives a brief introduction to the model and the numerical experimental strategy. The simulation results are presented in section 3. Finally, concluding remarks are given in section 4.

2. Model description and experimental strategy

2.1 *Regional climate model description*

The $P-\sigma$ regional climate model that was used in this study was developed from a five-layer model that was first designed by Kuo and Qian (1981, 1982). The model involves nine vertical atmospheric layers. The pressure coordinate was used above 400 hPa with four uniform layers. Below 400 hPa, σ and σ_B coordinates were used. Four σ layers were uniformly divided with $\Delta\sigma = 0.25$, and only one layer was defined in the σ_B coordinate with a 50-hPa thickness. A spherical grid system with a $1^\circ \times 1^\circ$ horizontal resolution was adopted, covering the region within 0°–60°N, 70°–140°E, where the complex surface topography was the dominant feature. The model includes a planetary boundary-layer parameterization, Kuo-type cumulus-convective parameterization scheme and a detailed atmospheric radiation process. There was also a two-layer soil model over land (Qian, 1988). The first soil layer represents the diurnal changes of the soil temperature and moisture, while the second layer depicts the annual changes. The soil temperature and moisture were calculated in each layer based on the soil thermal-conductive and the soil water-conservation equations. The surface temperature, latent heat and sensible heat fluxes could also be acquired. The time integration scheme was a one-hour Euler backward difference that was alternated with a five-hour central difference. The integration time-step was three minutes. The model's detailed performance and description were previously introduced by Qian (1985) and Wang and Qian (2001).

2.2 *Sub-grid orographic parameterization scheme*

The parameterization scheme accounting for the thermal effects of the sub-grid scale orography, which was incorporated into the $P-\sigma$ regional climate model, mainly included the impact that the sub-grid scale orography had on the surface solar and downward long-wave radiative fluxes, as well as on the surface sensible and latent heat fluxes. The terrain slope and orientation data that was used in this scheme was determined from the Earth Topography and Ocean Bathymetry Database (ETOPO5) that was collected with temporal resolution of 5 min. More details about the scheme are described by Zhang et al. (2006) and Zhu and Zhang (2005).

2.3 *Numerical experiments*

Two experiments were performed in this study:

(1) The control experiment (CTR): the sub-grid orographic scheme was not introduced.

(2) The sensitivity experiment (NEW): the sub-grid orographic scheme described above was included in the model

Three heavy rainfall events occurred during the period between 18 and 26 May, 2 and 19 June and 30 June to 12 July 1991, respectively. Two group experiments were designed to start and continue on from the beginning of each rainfall event until the end, in an effort solely to simulate the three heavy rainfall

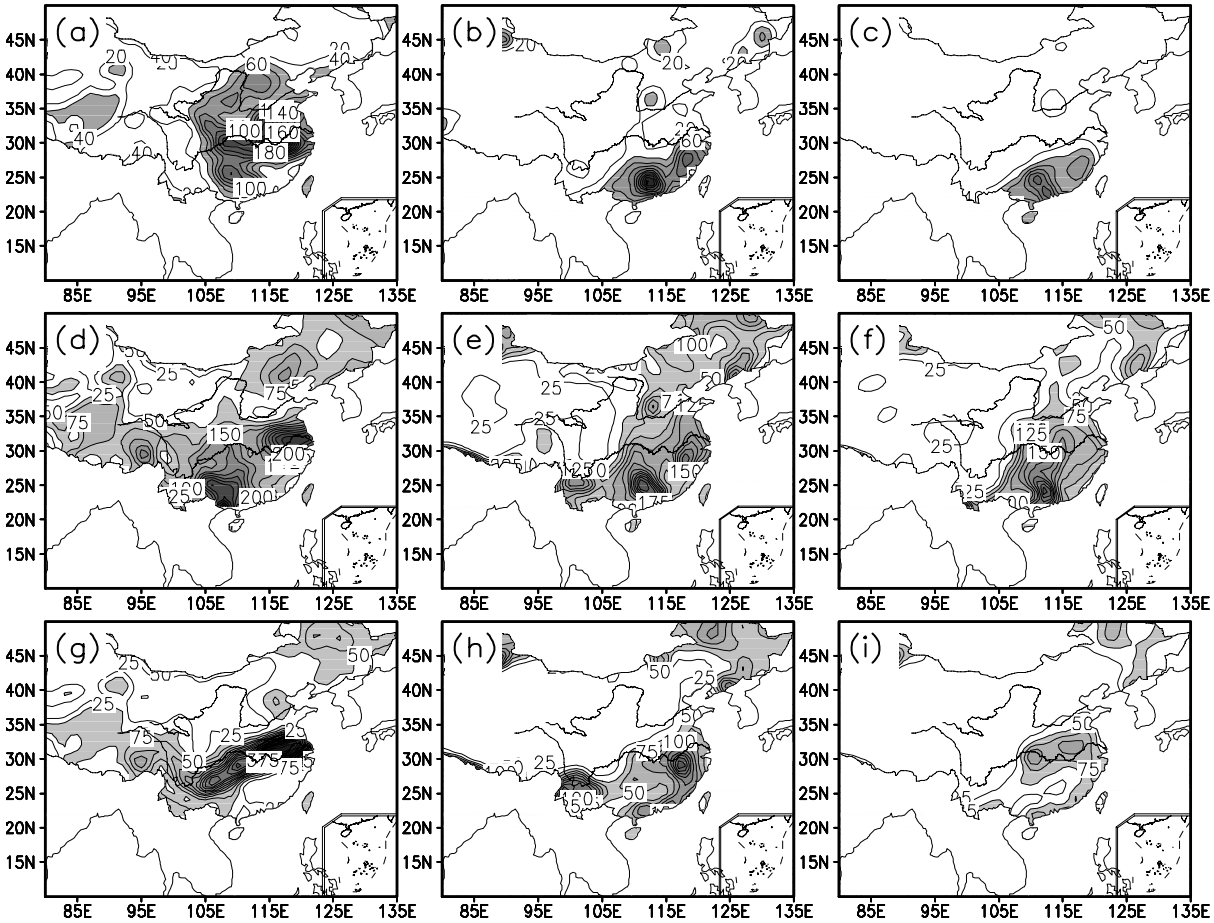

Fig. 1. The precipitation distributions for the (a, b, c) first, (d, e, f) second and (g, h, i) third heavy rainfall events in experimental observations (left), NEW (middle) and CTR (right), (units: mm).

events. The initial and lateral boundary conditions were provided by National Centers for Environmental Prediction/National Center for Atmospheric Research (NCEP/NCAR) reanalysis data at 6-hour intervals, that included the wind, air temperature, specific humidity and geopotential height fields. The weekly NCEP/NCAR reanalysis SST data was interpolated into the daily SST linearly and was taken as the oceanic boundary forcing.

3. Analysis of the simulation results

3.1 *Simulation of the three heavy rainfall events*

The rainfall events that occurred over the Yangtze-Huaihe River valley during the summer of 1991 have been extensively addressed by Ding (1993). They are unique in several aspects, such as the active mesoscale activities, the heavy rainfall that covered a large area, and the persistent heavy rainfall that was observed throughout June and July (Wang et al., 2000). There were three heavy rainfall events during that summer monsoon season of 1991, the first event extending from 18 to 26 May, the second from 2 to 19 June and the third from 30 June to 12 July. The associated atmospheric conditions, including the vertical motion, moisture condition, geopotential height and the temperature lapse rate in the simulation results, were investigated thoroughly. The differences between the two experiments, CTR and NEW, are then fully discussed in this section, due to their demonstration of the importance that the sub-grid scale orography's effects had upon the model-simulated rainfall. The observed rainfall in this section was calculated using the daily data that was provided by the World Meteorological Organization (WMO) surface networks, which has 714 stations in China.

3.1.1 *The first rainfall event*

The first heavy rain event occurred from 18 to 26 May 1991. The observations shown in Fig. 1a show that two notable rainbelts were located in the Yangtze-

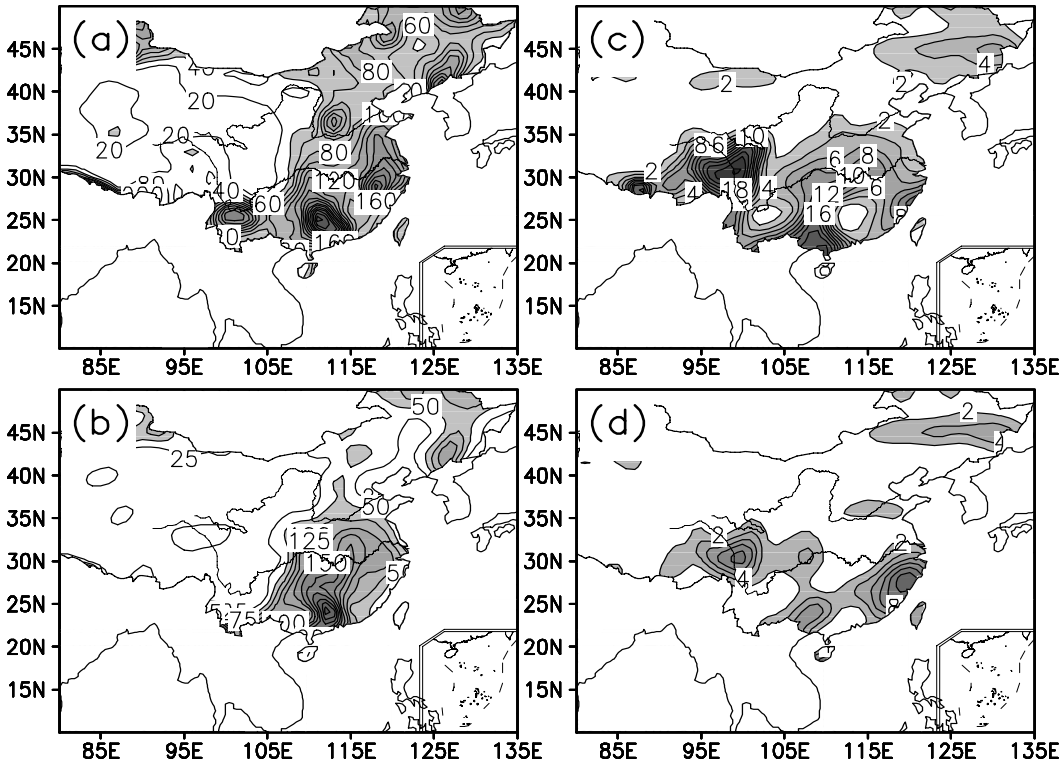

Fig. 2. The (a, b) convective and (c, d) large-scale precipitation distributions of the second heavy rainfall event in NEW (upper panels) and CTR (lower panels), (units: mm).

Huaihe River valley at the time. One rainband had a rainfall center that extended from Jiangsu Province into the northern region of the Jiangxi Province, which are located in the lower reaches of the Yangtze River valley, with a maximum precipitation of 180 mm being observed. The other extended from Lianyungang into Xuzhou, which is located in Jiangsu Province. The simulations of the first rainfall event for both the NEW and CTR schemes are presented as Figs. 1b and 1c, respectively. It was discovered that both experiments failed to reproduce the rainbelt located in northern Jiangsu Province and the rainfall center that was located along the Yangtze River valley was not captured very well. In both experiments, the rainfall centers were located near 27°N, 118°E, which was a lower latitude in comparison to the observations. The maximum precipitation for this rainfall center using NEW was near 100 mm, which was much lower than the observations, but still slightly higher than that simulated using CTR.

3.1.2 *The second rainfall event*

The second heavy rain event, which featured a continuous rainfall characteristic, extrended from 2 to 19 June. Fig. 1d gives the observed precipitation distribution during this period. It was shown that there was a heavy rainfall region located over Anhui, Jiangsu, and the northern Zhejiang Province, with a maximum precipitation of 225 mm being observed. There was also a 200 mm rainfall center located in southern China. The corresponding simulation results are shown in Figs. 1e and 1f, respectively, where it can be seen that the CTR scheme failed to reproduce the rainfall center in the lower reaches of the Yangtze River valley, while the simulation using the NEW scheme agreed well with the observations shown in Fig. 1d, although the location of the rainfall center was somewhat displaced in the lower latitudes. The simulated maximum precipitation in the lower reaches of the Yangtze River valley in NEW was 175 mm, which was about 50 mm lower than the observation. Furthermore, NEW simulated the precipitation over the other regions in China quite well.

3.1.3 *The third rainfall event*

After a short break during the middle of June, the heavy precipitation resumed at the end of June and continued into mid-July. Figure 1g shows the spatial distribution of the third event rainfall during the period between 30 June and 12 July. The observed precipitation along the entire Yangtze River valley during this event enhanced dramatically compared with the previous two events. The entire rainbelt, including a rainfall center over the Anhui and Jiangsu Provinces,

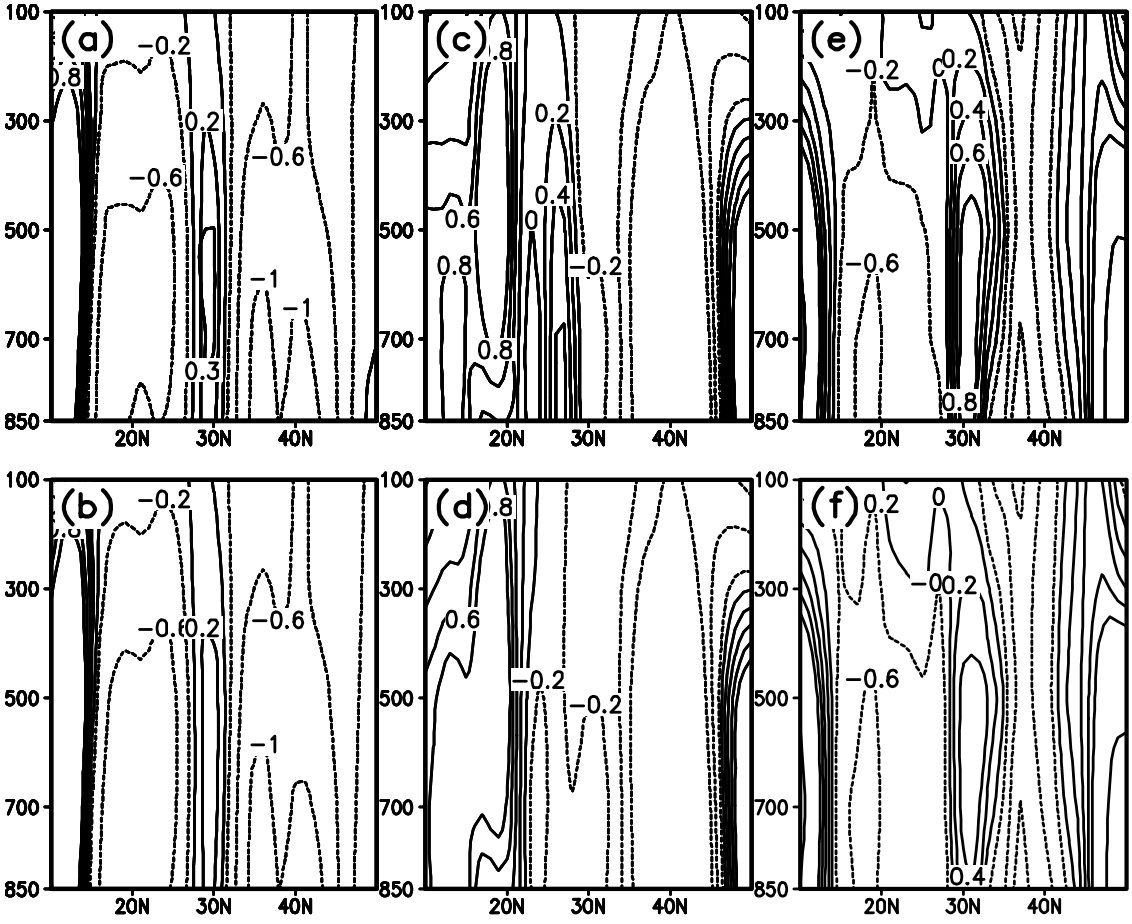

Fig. 3. The latitude-height distributions of the mean vertical velocities (units: 10^{-2} m s^{-1}) averaged over the region extending from 115°E to 120°E from the (a, b) first, (c, d) second and (e, f) third heavy rainfall events using NEW (upper panels) and CTR (lower panels) schemes.

was oriented from the northeast-southwest and almost covered the entire middle and lower reaches of the Yangtze River valley. The maximum precipitation for this rainbelt exceeded 425 mm. Figs. 1h and 1i provides the simulated precipitation using the NEW and CTR schemes. The rainbelt in the lower reaches of the Yangtze River was weakened using the CTR schemes, with a maximum precipitation of less than 100 mm, and the west side of the rainbelt reached into Hubei Province. A rainbelt clearly appeared in the same area using the NEW scheme, but its west side extended into southwestern China and the maximum precipitation of the rainbelt along the Yangtze River valley was close to 175 mm, which was weaker than the observation, but still larger than the results from CTR. Though the simulated rainbelt in NEW seemed to be broken, due to the discontinuity of the 75 mm precipitation isoline, its spatial distribution and orientation were closer to the observations than the results from using CTR. When compared with CTR, it was also found that the simulated precipitation over northeastern China and other areas of China in NEW was improved to a certain extent.

To provide a more quantitative comparison as to how much the simulated precipitation was improved, the mean precipitation over eastern China (25°–35°N, 115°–122°E) in the three rainfall events were calculated and are listed in Table 1. It is noted that the simulated rainfall in NEW were higher than those in CTR and were closer to the observations. The above analysis demonstrates that the model with the subgrid scale orographic scheme provides improved performance in simulating the precipitation distributions of these three heavy rainfall events, most especially in the second and third processes. However, when compared with the observations, there are still some deficiencies in the simulation results from NEW. For example, the precipitation in the lower reaches of the Yangtze River valley was generally underestimated by the model and the location of the rainfall center was typically had a southward shift. Meanwhile, it was found that the simulated precipitation over southern China during

Table 1. The mean rainfall averaged over eastern China for simulations using the NEW and CTR schemes in comparison to the observations. (units: mm).

	NEW	CTR	Observations
The First heavy rainfall event	19.9	12.9	64.1
The second heavy rainfall event	141.0	85.1	149.6
The third heavy rainfall event	103.8	37.1	177.2

the third rainfall event was stronger than the observations.

3.2 *Simulation of the vertical motion and moisture conditions*

Figure 2 shows the spatial distribution of the cumulus convective and the large-scale precipitation from the second heavy rainfall event. As shown in Fig. 2, the convective precipitation distribution and the amount simulated in both experiments were quite similar to the total observed precipitation, while the large-scale precipitation amount was small. Due to the similarity with the second event, the spatial distribution of the convective and large-scale precipitations from the first and third events are not shown in this paper.

It is evident in Fig. 2 that the rainfall was mainly caused by cumulus-convective precipitation. Therefore, it is necessary to investigate the reasons that result in the deficiencies of the convective-precipitation simulation. Vertical motion and moisture conditions are the key factors determining convective rainfall formation. Thus, in the following sections, comparisons of the two experiments with the NCEP/NCAR reanalysis that were carried out for these two aspects in an attempt to evaluate the simulation results and to find out the reasons that cause the deviations in the simulated precipitation using the NEW scheme, are discussed.

3.2.1 *Simulation of the vertical velocity and convergence at 850 hPa*

Figure 3 presents the height-latitude distributions of the simulated vertical velocities that were averaged from 115°E to 120°E. These cross-sections were taken through the longitudinal belt where the distribution and intensity of the precipitation, simulated in the two experiments, had the most remarkable differences. Therefore, the following discussions will concentrate on this longitudinal zone.

The observed rainfall center of the first precipitation event within this longitudinal zone was located at about 30°N (Fig. 1a). Correspondingly, a strong ascending motion and low-level convergence should have accompanied the rainfall center. However, as shown in Figs. 3a and 3b, the strong ascending motions that were simulated in both experiments were located at about 27°N, while the simulated vertical motions at 30°N were very weak, thus leading to the simulated heavy precipitation over South China (Figs. 1b and 1c). Figs. 4a–c display the convergence distributions of the areas where the convergence intensity was less than -3×10^{-6} s^{-1} at 850 hPa for the first heavy rainfall event. It indicates that the simulated convergence center using the NEW scheme was located at approximately 25°N and was a lower latitude when compared with the NCEP/NCAR reanalysis data, quite similar to the associated rainfall behavior also simulated with this scheme. However, the CTR scheme failed to reproduce this observation. In the first precipitation event, the stronger ascending velocity and low-level convergence in NEW were strongly associated with the heavier rainfall center when compared with those from CTR.

In the second precipitation event, the strong ascending motion simulated using the NEW scheme was located in the area between 25°–29°N, corresponding well with the location of the simulated rainfall center (Fig. 3c). The related convergence area, with a central intensity of -3×10^{-6} s^{-1} that is shown in Fig. 4e, was wider than the one simulated using the CTR scheme. Conversely, CTR generated a sinking motion between 25°N to 30°N, as shown in Fig. 3d. The rationality and accuracy of NEW in simulating the latitudinal locations of the ascending motion and the distribution of low-level convergence led to the reasonable simulations of the location and intensity of the rainfall center in the lower reaches of the Yangtze River valley that were obtained, which were not reproduced well in CTR experiments.

Figures 3e and 3f provide the simulated distributions of the vertical velocity during the third rainfall event using the NEW and CTR schemes, respectively. The simulated ascending motions were located in the longitude belt of 26°–35°N, with a strong ascending motion appearing in NEW. The comparison between these two experiments and the NCEP/NCAR reanalysis of the spatial distribution of the convergence field at 850 hPa, as shown in Figs. 4g–i, indicate that both experiments were successful in simulating the convergence zones that were located along the Yangtze River valley and corresponded well with the simulated distribution and orientation of the rainbelt, however, both were discontinuous. Compared with CTR, the convergence zone simulated in NEW was broader and more continuous. This led to the formation of an obvious rainbelt along the Yangtze River valley in NEW, which

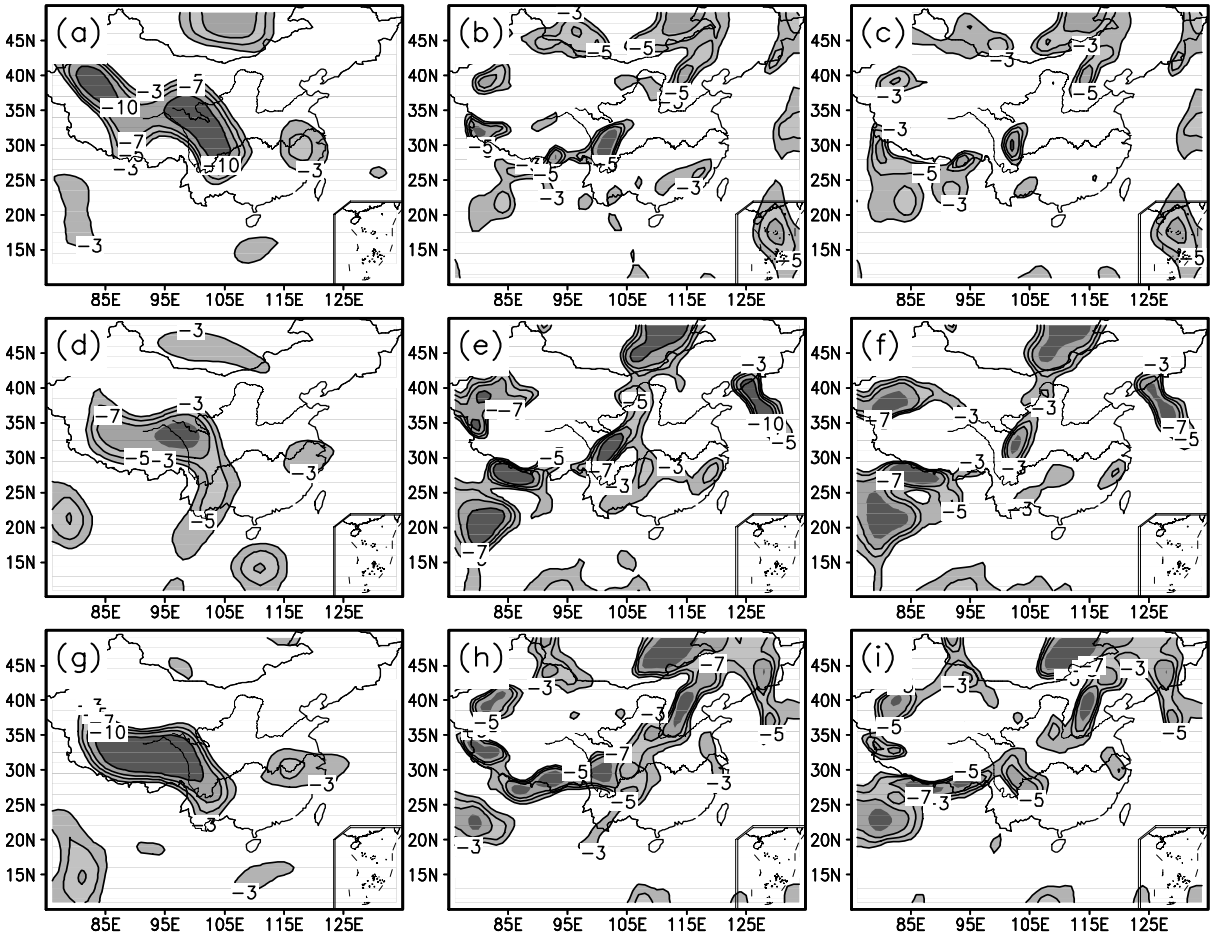

Fig. 4. The mean convergence (units: 10^{-6} s^{-1}) distribution at 850 hPa during the (a, b, c) first, (d, e, f) second and (g, h, i) third heavy rainfall events in NCEP/NCAR reanalysis (left), NEW (middle) and CTR (right). The shaded contours signify regions with convergences less than -3×10^{-6} s^{-1}.

was in good agreement with the observed precipitation.

In general, the apparent improvements in simulating the location of the rainfall center, as shown in the second precipitation event especially, was strongly attributed to the improved simulation of the vertical motion and convergence zone using the NEW scheme. Compared with CTR, NEW reproduced the precipitation patterns (orientation, magnitude and location) much better for the second and third events, due to its stronger ascending motion and broader convergence areas. Furthermore, these results indicated that the NEW scheme also provided an improved performance in simulating the vertical motion field in comparison to the CTR scheme. Obviously, there are also deficiencies in the simulated results in the NEW experiment. The intensity of the convergence area at 850 hPa in the lower reaches of the Yangtze River valley was weaker, and its location and spatial distribution were different from the NCEP/NCAR reanalysis data, thus yielding a slight mismatch between the simulated and observed precipitation patterns.

3.2.2 *Simulation of moisture distribution, transport and convergence*

Figure 5 shows the spatial distribution of the atmospheric moisture at 500 hPa during the first heavy rain event. It indicated that the observed moisture center was located over the lower reaches of the Yangtze River valley, while it was simulated, both with and without the sub-grid scale topography scheme, to be located over the Indo-China Peninsula. Futhermore, the simulated moisture at 500 hPa in the two simulation experiments were larger than in the observations. It was found that the values for the atmospheric moisture in the NEW experiment were the largest. A similar situation appeared in the second and third heavy rainfall events as well (not shown).

Figure 6 displays the transport and convergence of the moisture during the three rainfall events. The

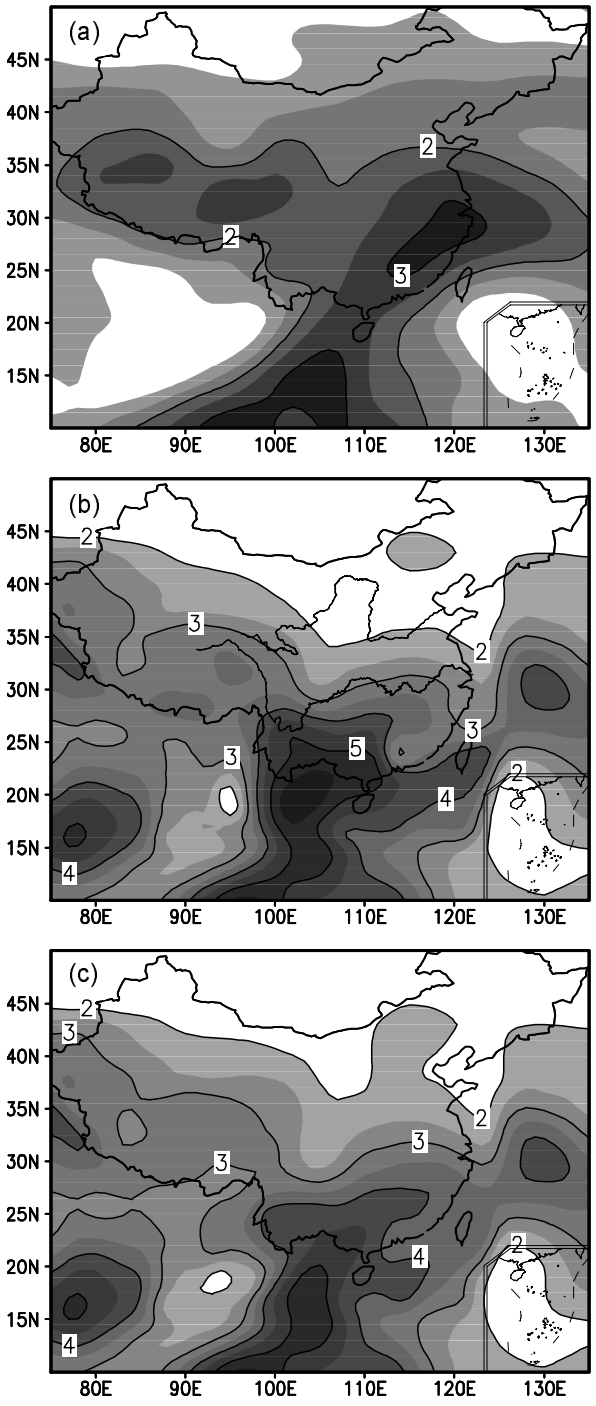

Fig. 5. The mean specific humidity (units: g kg^{-1}) distributions at 500 hPa from the first heavy rainfall event in (a) NCEP/NCAR reanalysis, (b) NEW and (c) CTR.

shaded areas represent that the convergence intensity was lower than -1.0×10^{-8} g s^{-1} cm^{-2} hPa^{-1}. As shown in Figs. 6a–c, the moisture simulated over the lower reaches of the Yangtze River in both experiments were mainly from the South China Sea in the first precipitation event, which agreed well with the NCEP/NCAR reanalysis data, however, the intensity of the moisture transport was weaker than in the NCEP/NCAR reanalysis data. The moisture convergence center in the NCEP/NCAR reanalysis data was located over the lower reaches of the Yangtze River valley, while the simulated centers in both experiments stayed further to the south, which was consistent with the simulated position of the rainfall center. Relative to CTR, the moisture convergence intensity in NEW was closer to the NCEP/NCAR reanalysis data and the distribution of the convergence area was broader, leading to the improvements in the simulated precipitation using the NEW scheme. Compared with the NCEP/NCAR reanalysis data, the intensity of the moisture convergence field that was simulated using NEW was subdued, which was conducive to the reduction in the rainfall amount.

In the second rainfall event, as shown in Figs. 6d, e and f, both the simulated moistures over the lower reaches of the Yangtze River valley came mainly from the South China Sea and the Bay of Bengal, which was quite similar to what was observed. The simulated moisture transport from the Bay of Bengal using CTR was weakened around the Tibetan Plateau, while the transport simulated using NEW was more reasonable. A moisture convergence center was located in the lower reaches of the Yangtze River valley using the NEW scheme, which was in good agreement with the NCEP/NCAR reanalysis data. It was also found that the CTR simulation also reproduced a moisture convergence region in the lower reaches of the Yangtze River valley, but its distribution was very narrow and its intensity was very weak, which may be the reason for the failure of CTR in reproducing the rainfall center over this region.

As illustrated in Figs. 6g–i, it was noted that the moisture located over the lower reaches of the Yangtze River valley from the NCEP/NCAR reanalysis data for the third precipitation event were mainly from the South China Sea. Meanwhile, the moisture from the Bay of Bengal was also important. The moisture simulated in CTR came mainly from the South China Sea and the moisture transport from the Bay of Bengal was very weak. However, the NEW scheme reproduced the moisture transport intensity and route more effectively than the CTR scheme. In both experiments, there are moisture convergence zones located along the Yangtze River valley, that corresponded to the location of the simulated rainbelts quite well. With the broader areas and the stronger intensity simulated using the NEW scheme in comparison with the CTR scheme, NEW simulated the spatial distribution of the moisture convergence reasonably well. According to the discussion

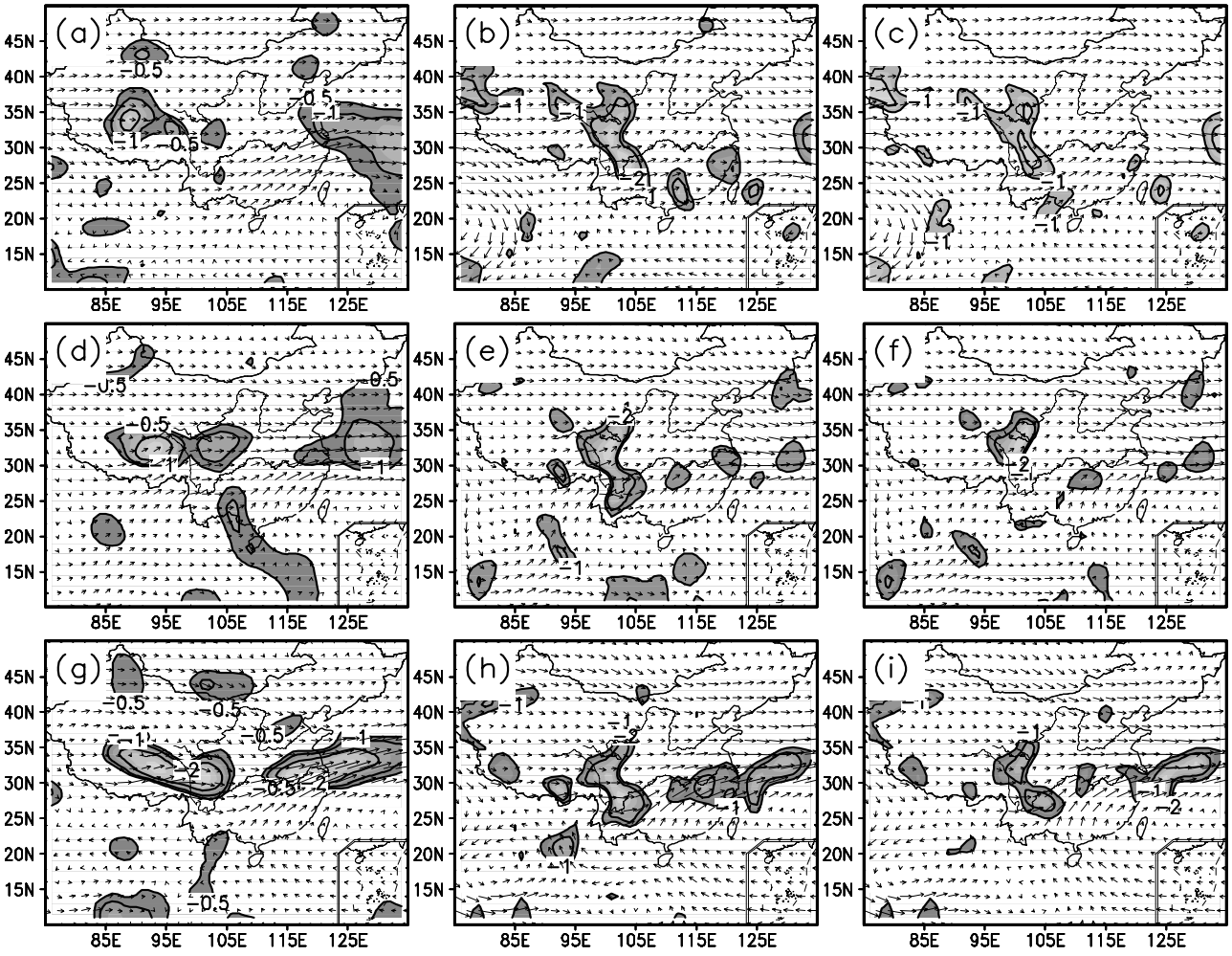

Fig. 6. The mean moisture transportation (units: g s^{-1} cm^{-1} hPa^{-1}) and convergence (units: 10^{-8} g s^{-1} cm^{-2} hPa^{-1}) intensity distributions at 500 hPa during the (a, b, c) first, (d, e, f) second and (g, h, i) third heavy rainfall events in NCEP/NCAR reanalysis (left), NEW (middle) and CTR (right). The nonuniform arrowhead length is used in representing the transportation intensity. Shaded contours signify regions with values less than -0.5×10^{-8} g s^{-1} cm^{-2} hPa^{-1}.

above, the improvement in the simulated precipitation that was observed in the NEW experiment, was in part due to the improved simulation of the moisture convergence pattern.

From the analysis above, it was determined that the simulated moisture transport and convergence fields in NEW at 500 hPa, especially during the second and third heavy precipitation events, were better than those from the CTR experiment. The more accurate and reasonable simulations of the moisture sources, transport and convergence intensities obviously led to the improved performance in the simulation of the precipitation using the NEW scheme in comparison with CTR. However, there are still some discrepancies between the simulated moisture transport and convergence intensity in NEW and the NCEP/NCAR reanalysis data. In addition, the moisture content at 500 hPa in NEW was larger than the NCEP/NCAR reanalysis data in each of the heavy precipitation events. The above analysis indicates that the deviations in simulations of moisture condition and vertical motion were clearly related to the deviations in simulation of the precipitation.

3.3 *Simulations of surface radiation, geopotential height and temperature lapse rate*

Referring to the studies by Zhu and Zhang (2005) and Zhang et al. (2006), we calculated the percentage of the mean surface solar and downward longwave radiation flux differences between the two experiments with and without the sub-grid orographic scheme. Here we only present the percentage distribu-

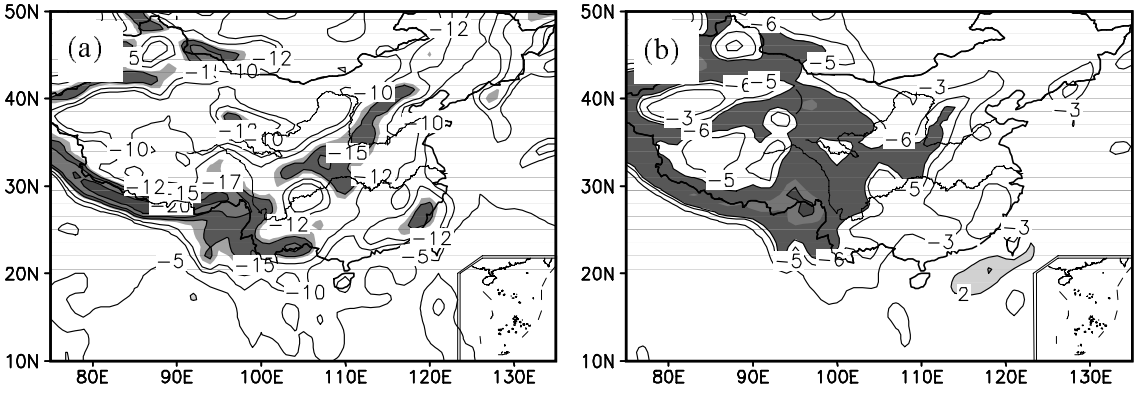

Fig. 7. The percentage distributions of (a) the surface mean solar and (b) downward long-wave radiation flux difference between the two experiments (NEW−CTR) in the second rainfall events.

tions for the second heavy rainfall event (Fig. 7). It was noted that the prominent changes in the surface solar radiation and long-wave radiation fluxes were located around the complex topographical regions of western China, especially towards the south and southwest edges of the Tibetan Plateau during the second rainfall event. The largest changes in the solar radiation and long-wave radiation fluxes appeared around the Tibetan Plateau. The sub-grid topography scheme reduced the absorbed solar radiation and long-wave fluxes at the earth's surface on the southern side of the Tibetan Plateau, with maximum reductions of 20% and 10%, respectively. These reductions led to changes in geopotential height field and atmospheric stratification conditions.

Figure 8 shows the evolution of the differences in the geopotential height and temperature lapse rate at 700 hPa between NEW and CTR during the second rainfall event, in the region from (25°N, 75°E) to (30°N, 125°E). Compared with CTR, the geopotential height at 700 hPa decreased in NEW, and the negative geopotential height difference at 700 hPa propagated northeastwards into eastern China over the entire event. In fact, the negative geopotential height difference at 700 hPa represents the strengthening of a low pressure system or the weakening of a high pressure system in NEW. At the same time, the temperature lapse rate at 700 hPa increased to the east of 100°E in NEW, indicating that the atmosphere was more unstable in NEW than in CTR. The temperature lapse rate changes also showed an eastward propagation feature, similar to the geopotential height changes. The sub-grid orographic scheme modified the surface energy budget, especially over the complicated terrain areas located in western China (in Fig. 7), leading to the development and eastward propagation of the negative geopotential height differences and unstable conditions in the lower atmosphere, which are in favor of the formation of convective precipitation. This is one possible reason for the observed improvements in the precipitation simulations of the lower reaches of the Yangtze River valley using the NEW scheme.

4. Concluding remarks

In this study, a parameterization scheme used to simulate the thermal effects of the sub-grid scale orography, was incorporated into the $P-\sigma$ regional climate model that was developed in Nanjing University in an effort to simulate the three heavy rainfall events that occurred along the Yangtze River valley during the mei-yu period of 1991. The results of the precipitation simulations and the deviations were analyzed in this paper. The inclusion of the sub-grid orographic scheme clearly improved the regional climate model's performance in simulating the rainfall amount and distribution over the lower reaches of the Yangtze River valley. Comparison analysis, performed on the aspects of the vertical motion and moisture condition, respectively, showed that the incorporation of the sub-grid orography also improved the performance of $P-\sigma$ model in simulating the location and intensity of the ascending motion and convergence areas at 850 hPa and the moisture convergence areas at 500 hPa in the lower reaches of the Yangtze River valley. These ameliorations were conducive to the improvements observed in the simulation of the precipitation. However, there were also some deviations in the simulations of the vertical motion and moisture condition, which were clearly related to the deviations in precipitation simulation. It was found that the sub-grid orography scheme obviously modified the surface solar and long-wave radiation fluxes. Analysis of the differences in the geopotential height and temperature lapse rate at 700 hPa between the two experiments within the region between (25°N, 75°E) to (30°N, 125°E) dur-

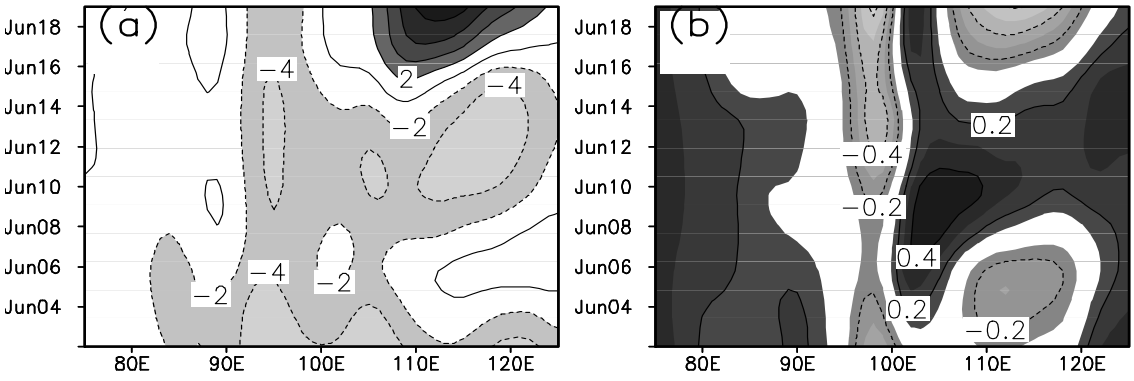

Fig. 8. The longitudinal-time cross-section of the geopotential height difference (a, units in m), temperature lapse rate (b, units in °C km^{-1}) at 700 hPa along the line from (25°N, 75°E) to (30°N, 125°E) between the NEW and CTR experiments during the second heavy rainfall event.

ing the second precipitation event, indicated that the change in the surface energy flux around the Tibetan Plateau, led to the development and eastward propagation of the negative geopotential height differences and the unstable conditions present in the lower atmosphere. This was due to the inclusion of the sub-grid orographic scheme. The sub-grid orographic thermal parameterization scheme changed the surface energy budget components and affected the precipitation simulation through the adjustment of the atmospheric circulation. This is a possible reason why the inclusion of the sub-grid orographic thermal parameterization scheme led to the observed improvements in the precipitation simulation in the regional climate model.

In this paper, the sub-grid orographic scheme was only introduced into the $P-\sigma$ regional climate model in an effort to evaluate the impact on the simulation of three heavy precipitation events that had occurred within the middle and lower reaches of the Yangtze River valley, implementation and verification of this scheme in other regional climate models and improvement and refinement to this scheme will be required in the future.

Acknowledgements. This study was jointly funded by the National Natural Science Foundation of China (Grant Nos. 40333026 and 40275032), and the National Key Scientific Research Plan (2001BA607B). We are very grateful for the use of the NCEP/NCAR reanalysis data. We appreciate the constructive comments and suggestions provided by the two anonymous reviewers, which greatly improved this paper.

REFERENCES

Ding, Y., 1993: *Research on the 1991 Persistent, Severe Flood over Yangtze-Huai River Valley*. China Meteorological Press, 255pp. (in Chinese)

Fu, B., 1983: *Climate in Mountainous Regions*. Science Press, Beijing, 270pp. (in Chinese)

Giorgi, F., 1997: An approach for the representation of surface heterogeneity in land surface models. Part I: Theoretical framework. *Mon. Wea. Rev.*, **125**, 1885–1899.

Giorgi, F., and R. Avissar, 1997: Representation of heterogeneity effects in earth system modeling: Experience from land surface modeling. *Rev. Geophys.*, **35**, 413–438.

Giorgi, F., R. Francisco, and J. Pal, 2003: Effects of a subgrid-scale topography and land use scheme on the simulation of surface climate and hydrology. Part I: Effects of temperature and water vapor disaggregation. *J. Hydrometeor.*, **4**, 317–333.

Ghan, S. J., X. Bian, A. G. Hunt, and A. Coleman, 2002: The thermodynamic influence of subgrid orography in a global climate model. *Climate Dyn.*, **20**, 31–44.

Kuo, H. L., and Y. Qian, 1981: Influence of the Tibetan Plateau on cumulative and diurnal changes of weather and climate in summer. *Mon. Wea. Rev.*, **109**, 2337–2356.

Kuo, H. L., and Y. Qian, 1982: Numerical simulation of the development of mean monsoon circulation in July. *Mon. Wea. Rev.*, **110**, 1879–1897.

Leung, L. R., and S. J. Ghan, 1998: Parameterizing subgrid orographic precipitation and surface cover in climate models. *Mon. Wea. Rev.*, **126**, 3271–3291.

Li, L., and B. Zhu, 1990: The modified envelope orography and the air flow over and around mountains. *Adv. Atmos. Sci.*, **7**, 249–260.

Li, Z., and D. Weng, 1987: A model to compute the terrain parameters in mountainous region. *Acta Geographica Sinica*, **42**(3), 269–274. (in Chinese)

Palmer, T. N., G. J. Shutts, and R. Swinbank, 1986: Alleviation of a systematic westerly bias in general circulation and numerical weather prediction models through an orographic gravity wave drag parameterization. *Quart. J. Roy. Meteor. Soc.*, **112**, 1001–1039.

Qian, Y., 1985: A five-layer primitive equation model with topography. *Plateau Meteorology*, **4**(2), 1–28. (in

Chinese)

Qian, Y., 1988: A scheme of calculation of heat balance temperature at ground surface. *Scientia Atmospherica Sinica*, **8**, 14–27. (in Chinese)

Qian, Y., 2000: Effects of the envelope orography and gravity wave drag on the climate modeling. *Quarterly Journal of Applied Meteorology*, **11**, 13–20. (in Chinese)

Qian, Y., and L. Dong, 1995: Effects of the envelope degree of orography on the simulated climate properties. *Acta Meteorologica Sinica*, **9**, 302–312.

Seth, A., F. Giorgi, and R. E. Dickinson, 1994: Simulating fluxes from heterogeneous land surfaces: explicit subgrid method employing the Biosphere-Atmosphere Transfer Scheme (BATS). *J. Geophys. Res.*, **99**, 18561–18667.

Wallace, J. M., S. Tibaldi, and A. J. Simmons, 1983: Reduction of systematic forecast errors in the ECMWF model through the introduction of an envelope orography. *Quart. J. Roy. Meteor. Soc.*, **109**, 683–718.

Wang, S., and Y. Qian, 2001: Effects of vertical resolution on the climate modeling in regional climate model. *Plateau Meteorology*, **20**(1), 28–35. (in Chinese)

Wang, W.-C., W. Gong, and H. Wei, 2000: A regional model simulation of the 1991 severe precipitation event over the Yangtze-Huai River valley. Part I: Precipitation and circulation statistics. *J. Climate*, **13**, 74–92.

Weng, D., W. Chen, J. Shen, and J. Gao, 1984: *Agricultural Microclimate*. China Agriculture Press, 99pp. (in Chinese)

Zhu, X., and Y. Zhang, 2005: Parameterization of subgrid topographic slope and orientation in numerical model and its effect on regional climate simulation. *Plateau Meteorology*, **24**(2), 136–142. (in Chinese)

Zhang, Y., A. Huang, and X. Zhu, 2006: Parameterization of the thermal impacts of sub-grid orography on numerical modeling of the surface energy budget over East Asia. *Theor. Appl. Climotol.*, **86**, 201–214. DOI: 10.1007/s00704-005-0209-1.